Experimental Neurology 229 (2011) 226–237

Contents lists available at ScienceDirect

Experimental Neurology

journal homepage: www.elsevier.com/locate/yexnr

In vitro modelling of Alzheimer's disease: Degeneration and cell death induced by viral delivery of amyloid and tau

Sandra Stoppelkamp, Helen S. Bell, Jon Palacios-Filardo [1], Derryck A. Shewan, Gernot Riedel, Bettina Platt *

School of Medical Sciences, College of Life Sciences and Medicine, University of Aberdeen, Institute of Medical Sciences, Foresterhill, Aberdeen AB25 2ZD Scotland, UK

ARTICLE INFO

Article history:
Received 2 December 2010
Revised 20 January 2011
Accepted 24 January 2011
Available online 2 February 2011

Keywords:
APP
Tau
Rat
Hippocampus
DRG
Calcium homeostasis
Culture
Drug testing

ABSTRACT

With increasing life expectancy, Alzheimer's disease (AD) and other dementias pose an increasing and as yet unresolved health problem. A variety of cellular models of AD has helped to decipher some key aspects of amyloid and tau related degeneration. The initial approach of extracellular applications of synthetic peptides has now been replaced by the introduction of amyloid precursor protein (APP) and tau genes. In the present study adenoviral transductions were exploited for gene delivery into primary rat hippocampal and dorsal root ganglion (DRG) cultures to enable comparative and mechanistic studies at the cellular level and subsequent drug testing. Time lapse experiments revealed a different pattern of cell death: apoptotic-like for APP whereas tau positive cells joined and formed clusters. Mutated human APP or tau expression caused accelerated neuronal damage and cell death (cf. EGFP: −50% for APP at 5 days; −40% for tau at 3 days). This reduction in viability was preceded by decreased excitability, monitored via responses to depolarising KCl-challenges in Ca^{2+} imaging experiments. Additionally, both transgenes reduced neurite outgrowth in DRG neurones. Treatment studies confirmed that APP induced-damage can be ameliorated by β- and γ-secretase inhibitors (providing protection to 60–100% of control levels), clioquinol (80%) and lithium (100%); while anti-aggregation treatments were beneficial for tau-induced damage (60–90% recovery towards controls). Interestingly, caffeine was the most promising drug candidate for therapeutic intervention with high efficacy in both APP (77%) and tau-induced models (72% recovery). Overall, these cellular models offer advantages for mechanistic studies and target identification in AD and related disorders.

Introduction

Alzheimer's disease (AD) is the most common type of dementia, and presents with progressive neurodegeneration, brain atrophy and cognitive impairment (Walsh and Selkoe, 2004). Currently, the over 35 million people affected worldwide (Querfurth and LaFerla, 2010) face few (symptomatic) treatment options. Accelerated research is therefore urgently needed, not only regarding advanced diagnostics, but also to identify treatment targets and determine cellular mechanisms. Studies of familial AD cases have identified mutations in the amyloid precursor protein (APP) and presenilins that cause built-up of toxic amyloid (Aβ) peptides (Selkoe, 2001), and are thus frequently used in transgenic models. Despite accumulation of insoluble plaques, small soluble aggregates of Aβ are now considered as the most harmful species (Mc Donald et al., 2010; Lesne et al., 2006; Cleary et al., 2005); both secreted forms and intracellular accumulation of Aβ are linked with early damaging processes (Kienlen-Campard et al., 2002; Hou et al., 2009). So far, no tau mutations have been identified in AD; but other tauopathies have revealed mutations linked with abnormal phosphorylation, reduced microtubuli binding and increased fibril formation (Goedert, 2005), causing microtubule and neurite destabilisation and impaired axonal transport (Niewiadomska et al., 2005; Paglini et al., 2000). Despite extensive research on the contribution of amyloid and tau towards AD, their interaction and impact on other disease markers are still poorly understood, though disturbed Ca^{2+} homeostasis is considered a common denominator (Stutzmann, 2007). Many *in vitro* studies have applied synthetic Aβ peptides, yet, naturally secreted forms appear considerably more damaging (Walsh et al., 2002). Thus, APP and tau expressing cell lines offer some advantages for early drug testing, but their altered cellular programmes and reduced sensitivity to toxic insults make data less physiologically relevant and transferrable than those obtained in primary neurones. To achieve transgene expression in

Abbreviations: AD, Alzheimer's disease; AdV, adenovirus; AICD, APP intracellular domain; APP, amyloid precursor protein; Aβ, amyloid beta; BACE1, beta-site APP cleaving enzyme 1; βCTF, beta-C-terminal fragment (of APP); BI, beta-secretase inhibitor; C99, C-terminal fragment; CBD, cell body diameter; CMV, cytomegalovirus; CQ, clioquinol; DAPM, N-[N-3,5-difluorophenacetyl]-L-alanyl-S-phenylglycine methyl ester (γ-secretase inhibitor XVI); DAPT, N-[N-(3,5-difluorophenacetyl)-L-alanyl]-S-phenylglycine t-butyl ester (LY-374973, γ-secretase inhibitor); DRG, dorsal root ganglion; GSK-3β, glycogen synthase kinase 3 beta; MB, methylene blue; MEM, minimal essential medium; NB, Neurobasal-A™; PKA, protein kinase A; sAPPα, soluble APP alpha.

* Corresponding author at: School of Medical Sciences, University of Aberdeen, Foresterhill, Aberdeen, AB25 2ZD, UK. Fax: +44 1224 555719.
E-mail address: b.platt@abdn.ac.uk (B. Platt).
[1] Present address: Instituto de Neurociencias de Alicante, UMH/CSIC, Av Ramon y Cajal s/n, 03550 San Juan de Alicante, Spain.

0014-4886/$ – see front matter © 2011 Elsevier Inc. All rights reserved.
doi:10.1016/j.expneurol.2011.01.018

primary neurones, viral vectors can be employed efficiently and elegantly. Especially for tau, which requires intracellular expression, this delivery method is essential and superior to invasive techniques such as direct injection or chemical transfection (Lo et al., 1994; Yuan et al., 1999). Adenoviral delivery of wild-type APP proved efficient in neurones, and resulted in increased sensitivity towards glutamate (low viral titers) or rapid cell death (high titers; Tominaga et al., 1997; Tominaga-Yoshino et al., 2001). Introduction of mutated APP_{swe} increased Aβ secretion in neurones and astrocytes (Macq et al., 1998), while transduction of APP_{ind} doubled the rate of cell death compared to wild-type APP in PC12 cells (Luo et al., 1999). Viral gene delivery was also implemented to selectively express Aβ intracellularly *in vitro* (Hou et al., 2009) and even utilised for *in vivo* studies (Masumura et al., 2000; Nishimura et al., 1998). In comparison, tau overexpression by adenoviral delivery caused axonal transport deficits in a neuronal cell line as well as in primary neurones (Stamer et al., 2002).

In the present study we systematically determined early (functional) and late (morphological) changes induced by viral delivery of mutated APP and tau transgenes, driven by the same promoter, in primary rat hippocampal and dorsal root ganglion (DRG) cultures to advance our mechanistic understanding of degenerative processes, and enable comprehensive assessments of treatment options.

Materials and methods

Adenoviral vectors

The cDNAs of two genes implicated in AD under control of the CMV promoter were fused to fluorophores and cloned into adenoviral vectors using the AdEasy™ system (Stratagene, UK). The human amyloid precursor protein (longest isoform, as APP770) containing the Swedish double mutation K670N/M671L, known to increase β-secretase cleavage (Citron et al., 1994), and the London mutation V717I (*$APP770_{swe/lon}$*), affecting γ-secretase cleavage thus increasing the proportion of $Aβ_{1-42}$ (Sinha and Lieberburg, 1999) (based on NM_000484.2) w C-terminally fused to EGFP and inserted into the AdEasy™ vector. For tau, the cDNA of the human tau splice variant 2N4R (based on NM_016835.2) harbouring a double mutation (*$tau_{P301L/R406W}$*) that decreases microtubule binding and increases heparin or arachidonic acid induced tau filament formation *in vitro* (Goedert, 2005), was fused to DsRed2 and inserted (constructs from genOway, France). For procedural controls, single fluorophore vectors were cloned as well. Sequence analyses (University of Dundee, UK) ensured correct in frame cloning.

Cell lines

Human (SH-SY5Y) and mouse (N2a, stably transfected with APP_{swe}) neuroblastoma cell lines were cultured in Dulbecco's Modified Eagle Medium (Sigma-Aldrich, UK) containing 10% foetal bovine serum, 2 mM L-glutamine, 100 U/ml penicillin and 100 μg/ml streptomycin (Gibco-Invitrogen, UK). SH-SY5Y cells were seeded at a density of 5×10^4 cells/cm^2 2 days prior to transduction with 1×10^7 IFU/ml and expression of the transgenes was controlled via visualisation of the fluorescent protein tags after 24 h.

Primary rat hippocampal culture preparation

Primary rat hippocampal cultures were prepared as described previously (e.g. Ryan et al., 2009; Koss et al., 2007) with minor amendments (see also Stoppelkamp et al., 2010), from 2 to 5 day old Sprague–Dawley rat pups in compliance with the Home Office Animals (Scientific Procedures) Act, 1986. Briefly, hippocampi were dissected and placed in ice-cold HEPES buffered solution (HBS; 130 mM NaCl, 5.4 mM KCl, 1.8 mM $CaCl_2$, 1 mM $MgCl_2$, 10 mM HEPES, 25 mM D-glucose — all compounds from VWR International, Poole, UK) pH adjusted to 7.4. Hippocampi were transferred to a protease solution (type X and type XIV, 1 mg/ml each in HBS, Sigma-Aldrich, Dorset, UK), chopped and enzymatically digested for 40 min at room temperature. After washing and repeated trituration in HBS the cells were resuspended in Minimal Essential Medium (MEM, Gibco-Invitrogen, UK) containing 10% FBS, 2 mM L-glutamine and plated onto poly-L-lysine coated cell culture dishes for 1 h at 37 °C 5% CO_2 in humidified atmosphere. Subsequently, Neurobasal-A™ (NB, Gibco-Invitrogen, UK) supplemented with 2% B27 (Gibco-Invitrogen, UK), 500 μM L-glutamine (Sigma-Aldrich, UK) and 10 ng/ml human basic fibroblast growth factor (Invitrogen, UK) was added. At 2 days *in vitro* (DIV) half of the medium was exchanged with NB 2% B27, 2 mM L-glutamine, 50 μM L-glutamate. Hippocampal cultures were transduced at 3 DIV with 4×10^6 IFU in 1 ml culture medium and incubated for 3 h at 37 °C, 5% CO_2 in humidified atmosphere. After primary viral incubation, additional (1 ml) medium was added. Cultures were left until experimentation at 37 °C, 5% CO_2, except for those including an intermitted wash (see below).

DRG cultures

Dorsal root ganglia (DRG) were isolated from 1–4 day-old Sprague–Dawley rats as described previously (Murray et al., 2009). Briefly, trimmed dorsal root ganglia were incubated in 10 U/ml papain-containing retinal buffer (200 μg/ml BSA, 1.65 μM D-L-cysteine, 5 mM HEPES, 16 mM D-glucose, 1.7 mM $CaCl_2$, 0.58 mM $MgSO_4$, 10.5 mM $MgCl_2$, 0.95 mM $NaHCO_3$, 20 mM KCl — dissolved in Hank's Balanced Salt Solution; containing phenol red) for 20 min at 37 °C followed by trituration in trypsin inhibitor (0.25 mg/ml; Sigma, UK)/DNase (50 μg/ml; Sigma, UK) solution. Dissociated neurones were suspended in modified Bottenstein and Sato's fluid supplemented with insulin (20 μg/ml; Sigma, UK), nerve growth factor (10 ng/ml; Serotec, UK), foetal bovine serum (2%, Biosera, UK) and basic fibroblast growth factor (5 ng/ml; Invitrogen, UK) and plated on polylysine (10 μg/ml) and fibronectin (5 μg/ml) coated coverslips at a density of 5000/ml. At 2.5 h (initiation of neurite outgrowth) or 24 h (maintenance of neurites) after plating, DRG cultures were transduced with 4×10^6 IFU in 500 μl culture medium and fixed 48 h later with 4% buffered paraformaldehyde for 10 min at room temperature.

Immunoblotting

Rat hippocampal cultures were transduced as described above, 48 h post transduction, cells were lysed with RIPA buffer (20 mM HEPES, 150 mM NaCl, 100 μM EDTA, 1% Igepal; pH = 7.6; all components from Sigma, UK) containing Complete™ protease inhibitors (Roche, UK). After 15 min incubation on ice the lysate was centrifuged (10,000 *g*) and the supernatant (soluble/cytosolic fraction) collected for protein analyses. Boiled 25 μg total protein (determined via BCA assay; Sigma-Aldrich, Dorset, UK) was separated on 4–12% gradient NuPAGE Bis–Tris gels (Invitrogen, UK) under denaturing conditions followed by transfer onto nitrocellulose membranes (0.45 μm pore size, Invitrogen, UK). Membranes were blocked in 1× TBST (50 mM Tris Base, 150 mM NaCl, 0.05% Tween 20) with 5% dried skimmed milk at 4 °C over night. Proteins were detected using primary antibodies in TBST plus 5% BSA and 0.05% NaAzide (APP blot: 6E10 1:500, Sigma, UK; tau blot: anti-Tau5 1:1000, Biosource, UK; loading control: anti β-actin 1:1000, Santa Cruz Biotechnology, Germany) for 1 h at room temperature followed by incubation with horseradish peroxidase-coupled anti-mouse or anti-rabbit IgG (1:10,000; Chemicon, UK) in TBST plus 5% dried skimmed milk. Immunolabelled proteins were visualised via enhanced chemiluminescence reaction (GE Healthcare Ltd., Buckinghamshire, UK). Resulting autoradiographs were scanned. As procedural control for APP, N2a cells, stably transfected with $APP695_{swe}$, were used.

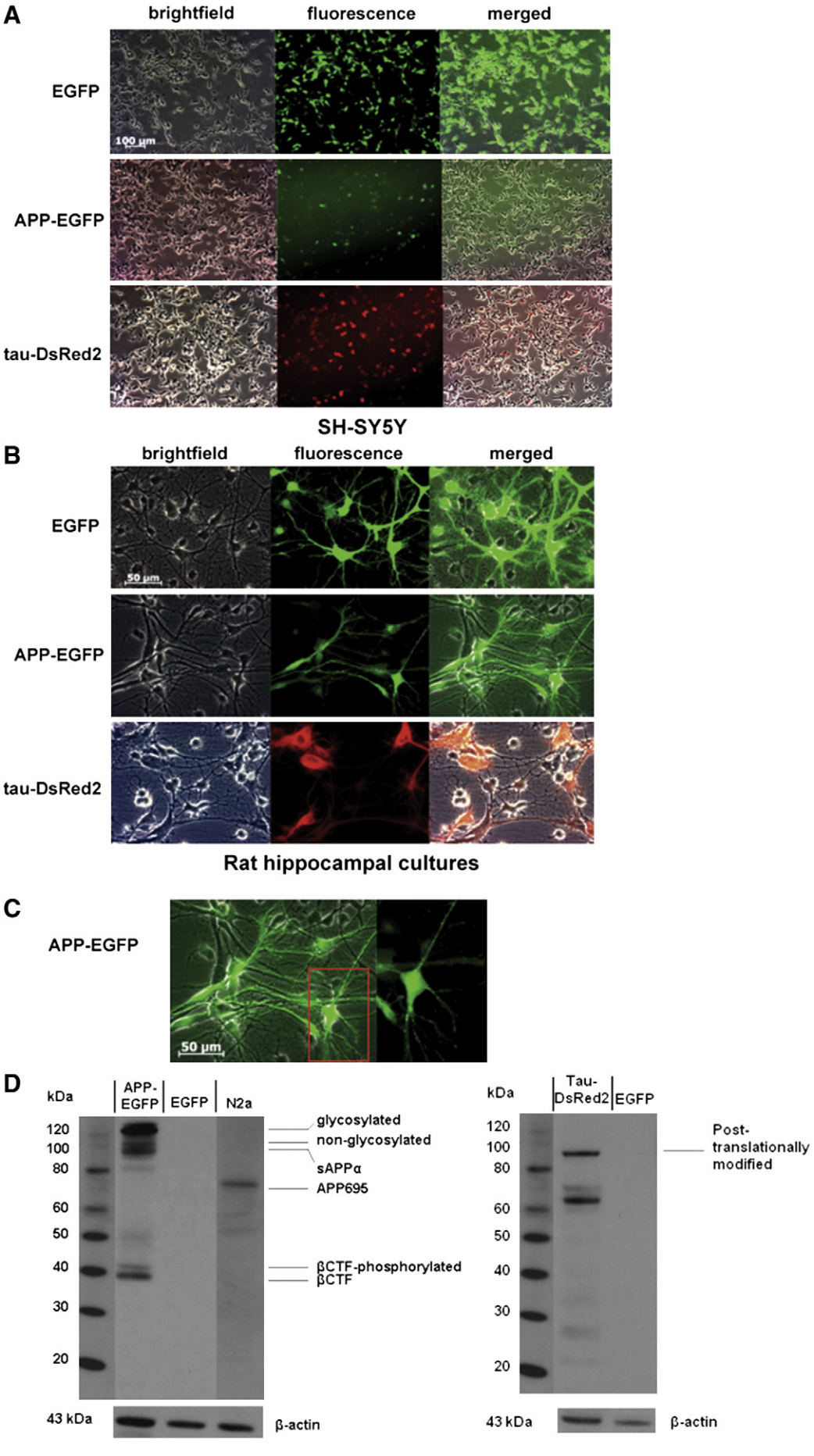
A
brightfield
fluorescence
merged
EGFP
APP-EGFP
tau-DsRed2
100 µm
SH-SY5Y
B
brightfield
fluorescence
merged
EGFP
APP-EGFP
tau-DsRed2
50 µm
Rat hippocampal cultures
C
APP-EGFP
50 µm
D
kDa
APP-EGFP
EGFP
N2a
120
100
80
60
50
40
30
20
glycosylated
non-glycosylated
sAPPα
APP695
βCTF-phosphorylated
βCTF
43 kDa
β-actin
kDa
Tau-DsRed2
EGFP
120
100
80
60
50
40
30
20
Post-translationally modified
43 kDa
β-actin

Time-lapse imaging

Hippocampal cultures were seeded on poly-L-lysine-coated glass bottom dishes (MatTek, USA). At 2 DIV the medium was exchanged with 2 ml phenol red-free NB (Invitrogen, UK; composition identical to its pH-indicator containing counterpart). At 3 DIV viral transduction was performed by addition of 4×10^6 IFU of the virus. After 24 h sterile HEPES-solution (pH = 7) was added to a final concentration of 15 mM to buffer the medium outside of the CO_2-adjusted atmosphere. The dishes were mounted in the heated chamber (37 °C) of the Leica AF6000 LX microscope with the CoolSNAP HQ system (Leica, Germany), fitted with a motor-controlled stage. Suitable areas were selected according to their density and presence of fluorescent neurones. Two different experimental setups were followed: long-term observation of several areas (6 to 7) per dish over 14–15 h with image acquisition every 10 min, or shorter observation over 4 h with image acquisition every minute. Both experiments were acquired using 20× magnification and 3×3 binning. The software and movable stage were used to identify the chosen regions exactly. Exposure times were adjusted to the initial brightness of the cells and kept constant throughout.

Fura-2 AM Ca^{2+} imaging

This followed our established protocol as described previously (Ryan et al., 2009; Koss et al., 2007). Briefly, 2 or 5 days post transduction (as specified below) hippocampal cultures were incubated for 1 h with the cell-permeable calcium indicator Fura-2 AM (10 μM; Invitrogen, UK). Dishes were mounted onto the stage of Olympus BX51 W1 microscope (Southall, UK) and an overlay of a fluorescent and brightfield picture was acquired with a digital CCD camera (Orca-ER; Hamamatsu, Japan) to identify transfected and non-transfected neurones. Cells were gravity-perfused with low Mg^{2+} HBS (130 mM NaCl, 5.4 mM KCl, 1.8 mM $CaCl_2$, 0.1 mM $MgCl_2$, 10 mM HEPES, 25 mM D-glucose, pH adjusted to 7.4) at a rate of 5 ml/min. All perfusion media contained 0.5 μM of the sodium channel blocker tetrodotoxin (Ascent-Scientific, UK) to prevent spontaneous cell firing and transmitter release. Ratiometric imaging was conducted using alternating excitation wavelengths (340 nm and 380 nm) from a Lambda DG-4 illumination system (Sutter Instruments, Novato, USA) and emission of Fura-2 was captured at 510 nm every 5 s. Baseline $[Ca^{2+}]_i$ levels were established for 5 to 10 min prior to 2 min application of 30 mM KCl in low Mg^{2+} HBS. Ratiometric values obtained from the Openlab acquisition software (V.4.02, Improvision, Coventry, UK) were plotted against time and the peak rise in $[Ca^{2+}]_i$ determined. Changes ≥ 0.04 (noise level) in fluorescence units were considered as responses. Responses of transduced neurones were calculated relative to non-transduced neurones (= intra-dish controls, in %). Experiments were repeated at least 3 times in independent cultures. The proportion of responding neurones was calculated separately for transduced and non-transduced cells and expressed as responder rates (RR). Statistical analyses were performed with Prism software (V5.02, GraphPad Software Inc., San Diego, USA) using an overall Kruskal–Wallis test followed by non-parametric Mann–Whitney *U*-tests for planned comparison of selected data pairs. $P<0.05$ was considered significant.

Long-term observation of transduced cultures and morphological scoring

Transduced hippocampal cultures were monitored over time in grid dishes (μ-Dish 35 mm, high Grid-500; Ibidi, Germany); high optical quality plastic bottom combined with the unique alphanumeric grid allowed the localisation and image capture of the same area within the dish under sterile conditions with an inverted fluorescent microscope (Axiovert S100 with AxioCam MRm and Axiovision release 4.7.2 software, Zeiss). On day 1 to 5 post transduction, 5 areas per dish were chosen and pictures taken daily with 10× objective magnification at fixed exposure times. Images were converted without alteration and aligned for comparison of the area density, the number of fluorescent cells, their intensity and fate. Changes in neuronal cell morphology were quantified using fluorescence imaging on live hippocampal transduced cultures. Before microscopic examination cultures were washed with pre-warmed HBS and visualised using a Zeiss microscope (Axioskop 2 plus) fitted with a digital camera (Axiocam) using Axiovision software (Zeiss, Hertfordshire, UK). Images taken at 40× objective magnification were manually counted for healthy, damaged and dead cells. Only neurones with smooth membranes, 3D appearance, long branched processes connecting with other neurones and the absence of vacuoles were considered as healthy. Subtle/early damage was determined based on reduced membrane smoothness, flattening of the cells and/or presence of vacuoles, but with processes still present. The criteria for late damage or dead cells were absence of processes and shrivelled membrane. Counts obtained from the 5 images per dish were pooled to yield one data point; at least 3 replications were conducted, each with 3 dishes per culture. Data are presented as percentage of healthy transduced neurones out of all transduced neurones. Statistical analyses were based on one-way analysis of variance (ANOVA) followed by planned paired comparisons using two-tailed Student's t-tests; $p<0.05$ was considered reliable.

Assessment of neurite outgrowth

At 48 h post transduction, DRG neurones were fixed and neurite outgrowth assessed (Murray et al., 2009; Murray and Shewan, 2008). Neurons with at least one neurite of 3 cell body diameters (CBD) in length were expressed as a percentage of the total number of neurons counted. This permitted us to assess the neurite outgrowth performance of each neurone, taking into account the wide variation in DRG neuronal soma size, in order to gain an overall appreciation of the neurite growth in each culture. Experiments were conducted at least 3 times from independent culture preparations. Statistical analyses were performed by one-way ANOVA followed by planned paired comparisons (two-tailed t-tests, significance set as $p<0.05$).

Drug treatments

Based on pilot studies to optimise treatment conditions, drugs were applied to hippocampal cultures 3 h post transduction; DRG cultures were treated at the time of viral transduction. Stock solutions of drugs were prepared in either DMSO or deionised water and stored at −20 °C. Working solutions were prepared freshly on the day to give final concentrations of 2 μM β-secretase inhibitor II (BI2, Calbiochem, UK; in DMSO) for treatment of hippocampal cultures and 700 nM BI2 for DRG, 50 nM β-secretase inhibitor IV (BI4, Calbiochem, UK; in DMSO), 50 μM caffeine (Sigma-Aldrich, UK; in water), 10 μM clioquinol (CQ, Sigma-Aldrich, UK; in DMSO), 1 nM compound E (Calbiochem, UK; in DMSO), 40 nM DAPM (N-[N-3,5-difluorophenacetyl]-L-alanyl-S-phenylglycine methyl ester; Calbiochem, UK; in DMSO), 1 μM DAPT (N-[N-(3,5-Difluorophenacetyl-L-alanyl)]-S-phenylglycine t-Butyl Ester; Sigma-Aldrich, UK; in DMSO) and 500 μM

Fig. 1. Expression analysis of the transgenes. (A) SH-SY5Y neuroblastoma cells transduced with 1×10^7 IFU/ml adenoviral vector, visualised 24 h post transduction. (B) Rat hippocampal cultures transduced with 2×10^6 IFU/ml, observed 48 h post transduction. (C) Close-up view of an APP-EGFP transduced neurone, identifying vesicular localisation of fluorophore-tagged APP. (D) Immunoblots (soluble fraction) of transduced hippocampal cell lysates (harvested 48 h post transduction). The mature (glycosylated) and immature (non-glycosylated) forms of APP-EGFP and phosphorylated tau-DsRed2 indicate correct post-translational modifications and cleavage products of APP (left) indicate correct processing. The APP blot was probed with anti-amyloid antibody clone 6E10, tau with anti-tau5; β-actin re-probing served as loading control. Stably transfected (APP695) N2a cells were used as a control for APP expression.

LiCl (Sigma-Aldrich, UK; in water). Treatment with methylene blue (MB; 0.02% final concentration, Sigma-Aldrich, UK) was carried out 1 day post transduction for 10 min at 37 °C, 5% CO_2 followed by two washes with pre-warmed HBS and subsequent incubation in culture medium until experimentation. This short-term incubation was conducted to prevent the photoreactive initiation of redox reactions of MB (Necula et al., 2007). All other treatments were maintained until microscopic examination or calcium imaging, washed cultures' refers to the introduction of a washing step 1 day post transduction performed as described for MB treatment to reduce the exposure to viral particles and wash off dead cells and debris. The final DMSO concentration did not exceed 0.02%; control experiments with 0.02% DMSO treatment cultures did not alter the percentage of morphologically healthy neurones and did not affect basal calcium homoeostatsis or potassium responses (data not shown, see also Ryan et al., 2009).

Results

Adenoviral gene delivery in neuroblastoma cells

The viral delivery system was initially tested in different cell culture systems to confirm expression and post-translational modifications (Fig. 1). Cellular localisation of the transgenic proteins was visualised by the fused fluorophores. In a human neuroblastoma cell line (SH-SY5Y) transgenic proteins were readily identified 24 h post transduction (Fig. 1A). As expected from the non-toxic small control protein, EGFP positive cells were more prominent in number and fluorescence intensity compared to APP and tau. This reflects the constitutive expression and relative stability of EGFP in the cells and confirms its non-toxicity (see below).

Transgene expression in rat hippocampal cultures

Since the scope of our *in vitro* approach was a primary neuronal model, viruses were subsequently applied to mixed rat hippocampal cultures optimised from previous studies (Stoppelkamp et al., 2010). Transgene expression was also readily detected in cultures 48 h post transduction via the fluorescent tag (Figs. 1B and C). Approximately 50–60% of the neurones were positive for the fluorescent control (EGFP) upon viral transduction, where the fluorescent protein was expressed throughout the cytoplasm and neurites. In APP-EGFP and tau-DsRed2 transduced cultures, slightly less positive neurones were achieved (~40%). At this early time point (48 h), an impact of tau but not APP expression on hippocampal morphology was already obvious (Fig. 1B bottom row), a first indication of a more aggressive tau-related pathology. Subsequent immunoblotting of transduced cultures with APP and tau specific antibodies verified the nature and processing of the transgenic proteins (Fig. 1D). The probing for tau revealed two bands (upper band: post-translationally modified tau) and no cross-reaction with endogenous tau at this antibody dilution (EGFP transduced cultures were negative). With 6E10, an antibody recognising amino acids 1–17 of the Aβ sequence, some of the APP metabolites were visualised; i.e. the full length protein, the soluble fraction after α-secretase cleavage (sAPPα) and the C-terminal region after β-secretase cleavage (βCTF) were identified in their immature and mature forms.

APP and tau cause neuronal cell death over 3 to 5 days

Further experiments were conducted in primary cultures only, owing to their closer relevance for *in vivo* conditions. The predominant vesicular localisation of APP (and/or its metabolites; see Fig. 1C) and the rapid movement we observed within cells is in accordance with previous observations (Goldsbury et al., 2006; Gralle and Ferreira, 2007), whereas the homogenous distribution of tau-DsRed2 throughout the soma and processes confirms its association with the cytoskeleton. A closer inspection of transduced rat hippocampal cultures over time revealed the earliest and most severe cell death in tau transduced cultures (from about 2–3 days post transduction), followed by APP transduced cultures (4–5 days) and little change in EGFP control cultures (Fig. 2). Cell clustering, observed only for tau positive cells (Figs. 1 and 2), indicated assembly and aggregation of tau-expressing cells. When observed over a period of 5 days, the number, density and intensity of fluorescent cells increased in EGFP controls. Viral transduction was performed on established cultures with existing extensive networks of neuronal processes, and EGFP expression did not markedly alter such features. In comparison, onset and progression of APP and tau expression was clearly detectable but less pronounced, with an increased proportion of dying and degenerating cells, as suggested by the decrease in overall cellular density (Fig. 2). The reduced expression is likely due to differing build-up of fluorescence-labelled proteins and

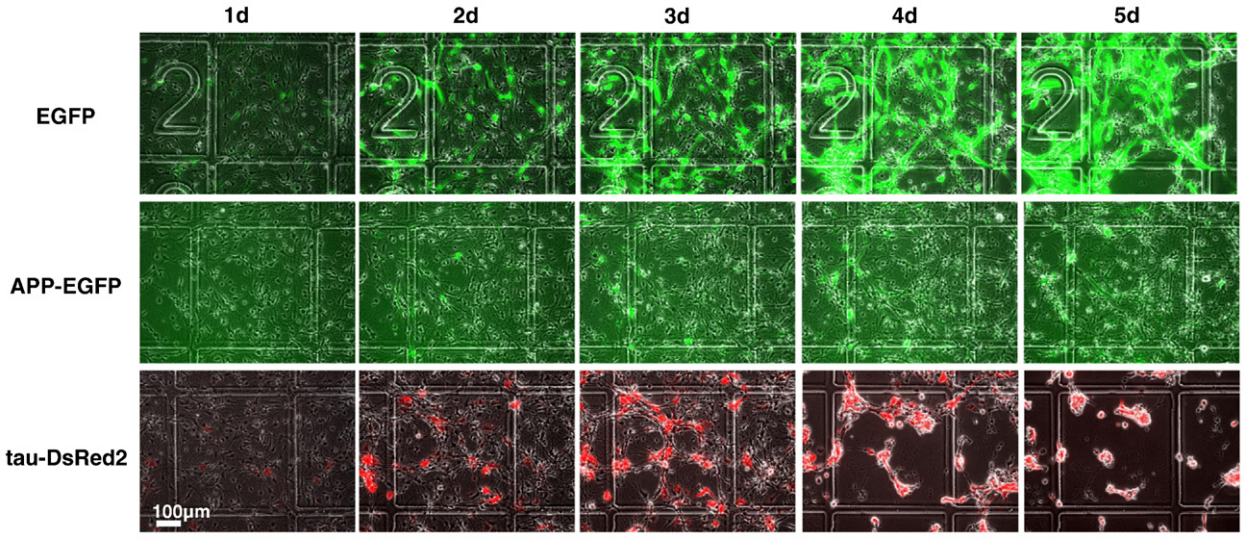

Fig. 2. Time course (1 to 5 days post transduction) of APP-EGFP and tau-DsRed2 expression in rat hippocampal cultures. Fluorescence and brightfield overlays of the same regions were acquired over 5 consecutive days. While density and fluorescence intensity increased in EGFP control transductions (upper panel) without adverse effects, APP-EGFP (middle) and tau-DsRed2 (bottom) transduced neurones had a higher rate of cell death, detected from disappearing fluorescent cells from the field of view. Tau-DsRed2 overexpression was not only harmful to the transduced cells but also spread to non-transduced neurones, resulting in a severe and progressive reduction of cell density. d = days post transduction; scale bar = 100 µm.

early stage toxicity. These initial observations guided the selection of suitable endpoints for early and late transgene-induced cellular alterations. For quantifications and treatments, intermediate time points were chosen before maximal pathological stages were reached, to provide an experimental window for bi-directional changes, i.e. potentially accelerated cell death or improvement with the treatments.

Visualising protein accumulation and degenerative events in APP and tau transduced neurones

Time-lapse imaging studies were performed on transduced neurones to gain an insight into the early impact of transgene expression on neuronal morphology, appearance and fate (Fig. 3). As procedural control, naïve cultures were investigated first, showing predominantly stationary neurones, progressively extending their neurites, though some somatic movement, proliferation and cell death were occasionally observed. Targeting the time of fluorescence onset (i.e. 24 h), APP-EGFP, tau-DsRed2 and EGFP transduced cultures were then compared. EGFP transduced cultures matched non-transduced controls, but cell death incidents increased in APP-EGFP and tau-DsRed2 transduced cultures (for quantification, see below). The majority of damaged cells disintegrated, detached and disappeared from the field of view (see video file 1). Contrary to expectations, the intraneuronal accumulation of APP-EGFP alone was not indicative of cell death onset (Fig. 3A), as it occurred in bright (yellow circle) as well as weak fluorescing (white and red circles) neurones at different times post transduction. APP-EGFP and tau-DsRed2 positive neurones also displayed different pathological characteristics: the withdrawal of neurites, continuing accumulation of fluorescent protein in the soma and subsequent disintegration of APP-EGFP positive neurones (Fig. 3B, see also video file 1) contrasted with swollen cell bodies after neurite withdrawal in tau-DsRed2 positive neurones and subsequent cell aggregation (Fig. 3C, see also video file 2) within the experimental time frame. As seen from the 5-day-observation (Fig. 2) ultimately most cells degenerated and eventually disappeared from the field of view.

Early functional changes of APP and tau pathology: impact on neuronal calcium homoeostasis and excitability

A hypothesis of AD onset (reviewed in Stutzmann, 2007) proposes abnormal intracellular calcium handling as an indicator of early pathology. We therefore compared neuronal excitability probed via potassium challenges between APP-EGFP, tau-DsRed2 and EGFP transduced cultures at 2 and 5 days post transduction (Fig. 4). Responses of non-transduced neurones in viral-treated dishes were found to be unaffected (data not shown) and responses of transduced neurones are thus expressed relative to those, as within experiment-control data.

Representative time courses of transduced neurones (Fig. 4A) illustrate reduced response size in tau-DsRed2 and APP-EGFP transduced neurones relative to EGFP. Pooled data indicated that basal intracellular calcium levels were elevated early (2 days post transfection) only in tau-DsRed2 positive neurones (Fig. 4B; $p = 0.004$) but not in APP-EGFP positive neurones. Nevertheless, introduction of APP-EGFP or tau-DsRed2 decreased neuronal calcium responses (by ~50% for APP-EGFP, $p = 0.03$, $n = 13$, and by ~75% for tau-DsRed2, $p = 0.001$, $n = 8$; Fig. 4C). Interestingly, at this early stage the responder rates of transgene positive neurones were similar between APP-EGFP, tau-DsRed2 and the EGFP controls, but the latter recovered to 79% 5 days post transduction, while a total loss of responsiveness in the remaining tau-DsRed2 positive neurones and a noticeable reduction (to 17%) in APP-EGFP positive neurones were observed (Fig. 4C). In the remaining responders, basal intracellular calcium levels were now also elevated (5 days post transduction, $p = 0.03$; Fig. 4B), supporting a progressive deterioration, alongside a ~93% reduction in intracellular calcium responses compared to the EGFP control ($p = 0.03$; Fig. 4C). Tau-transduction again showed a more aggressive profile beyond the already elevated basal intracellular calcium levels, with a stronger decline in evoked responses and eventual complete loss of excitability, matching our previous observations (see Fig. 2). Therefore, a 2 day post transduction time point was selected for proof-of-principle treatment studies. Here, β-secretase inhibitor II (BI2) treatment recovered calcium responses in APP-EGFP dishes ($p = 0.03$ cf. untreated APP-EGFP, $n = 5$; Fig. 4C) towards EGFP control levels ($p > 0.05$

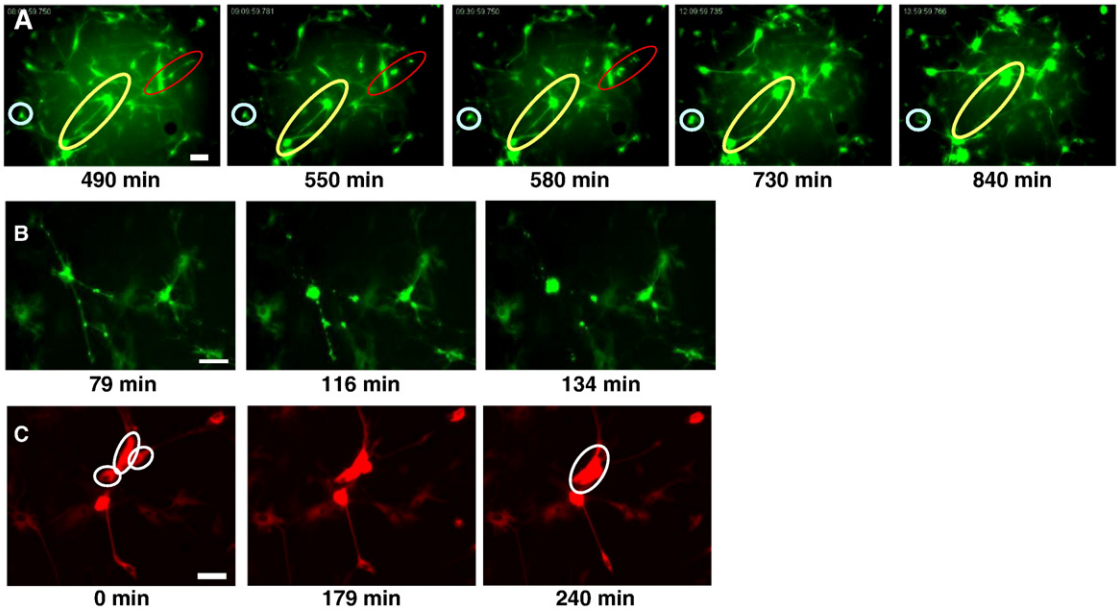

Fig. 3. Time-lapse imaging of APP-EGFP and tau-DsRed2 transduced neurones (24 h post transduction). (A) The accumulation of transgenic APP-EGFP in neurones did not correlate with cell viability. In the sample shown, neurones with lower fluorescence intensity (circled, left and right) died earlier than the brighter fluorescent neurone (centre). (B) APP-EGFP and (C) tau-DsRed2 positive neurones demonstrated different patterns of cell death: neurite withdrawal and disintegration in APP-EGFP neurones (B) and cluster formation in tau-DsRed2 positive neurones (C, circled). Scale bar: 50 μm. Times indicated are relative to the start of image acquisition (0 min=24 h post transduction). See also online supplement for corresponding videos.

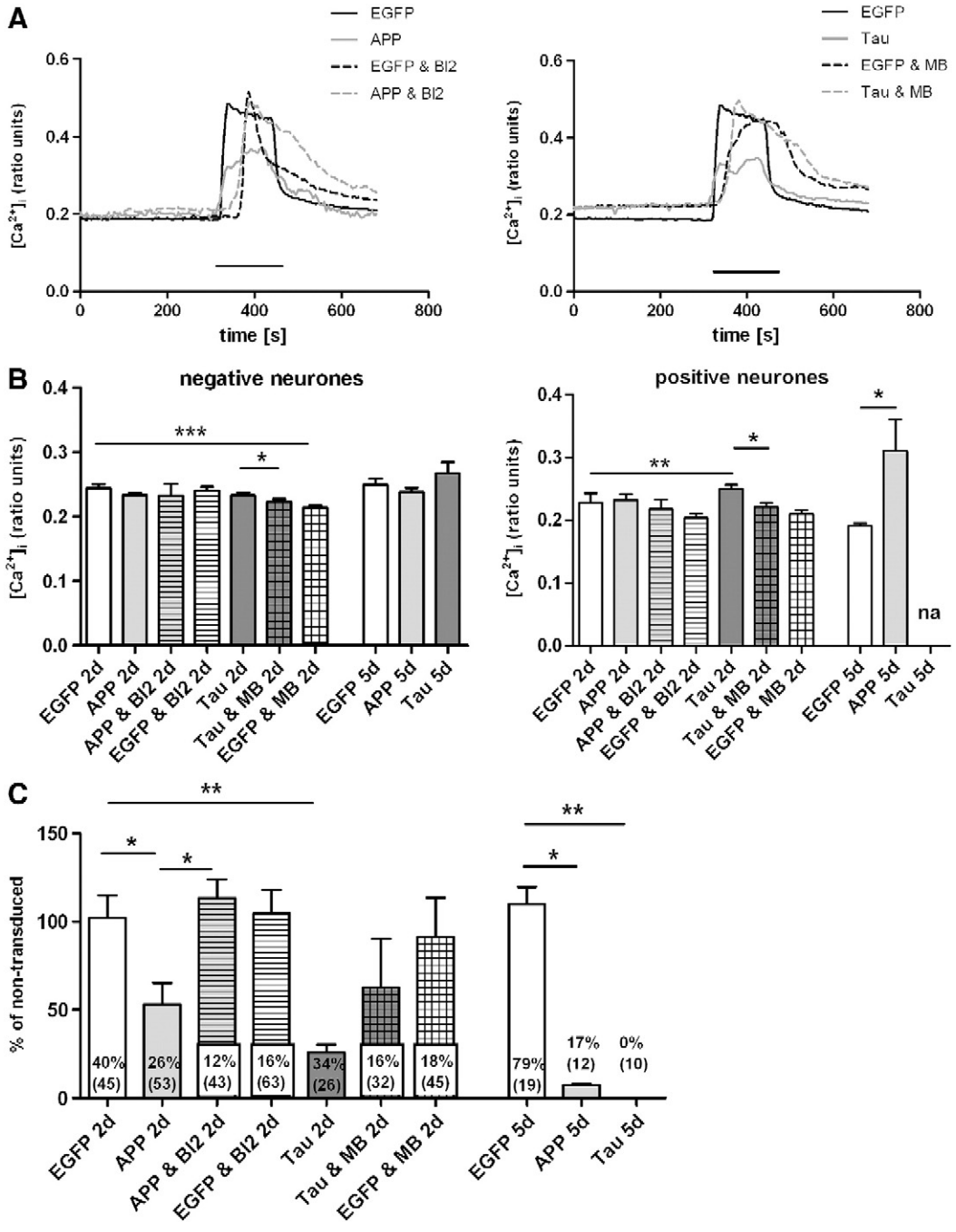

Fig. 4. Alterations in calcium homoeostasis indicate early stage damage. (A) Experimental time courses presented as mean values from 3 selected responding neurones. The bar indicates application of depolarising KCl solution. (B) Basal $[Ca^{2+}]_i$ in APP-EGFP transduced cultures did not differ from controls (negative neurones: non-transduced, positive neurones: transduced). Elevated $[Ca^{2+}]_i$ observed in tau-DsRed2 transduced neurones (positive and negative) was reduced by MB treatment. (C) APP-EGFP and tau-DsRed2 expression reduced neuronal excitability 2 days post transduction. Early changes in calcium signalling induced by APP-EGFP were reversible by β-secretase inhibition; MB treatment only yielded a trend towards amelioration in tau-DsRed2 positive neurones. Data are presented as percentage $[Ca^{2+}]_i$ change upon depolarising KCl application relative to non-transduced neurones of the same culture (+SEM). Responder rates (in %) are also given per condition together with the total number of neurones (in brackets). $^{*}p<0.05$; $^{**}p<0.01$; $^{***}p<0.001$. 2d = 2 days post transduction; 5d = 5 days post transduction; na: not analyzed; BI2 = β-secretase inhibitor II; MB = methylene blue.

cf. EGFP controls), indicating intracellular Aβ as cause of the altered calcium response, whereas methylene blue (MB) treatment (n = 5) only showed a non-significant trend for improvement in tau-DsRed2 dishes. Intriguingly, MB treatment could recover the elevated basal intracellular calcium levels of tau-DsRed2 positive neurones to EGFP control levels (Fig. 4B). The adjustment of basal calcium values was also seen for tau-DsRed2 negative neurones, suggesting a general effect of MB on calcium homoeostasis not specific to the tau transgene.

Late stage damage: morphological scoring for quantification of treatment success

While calcium imaging yielded information for early functional changes upon transgenic APP and tau overexpression, the severity of changes and complexity made this approach unsuitable for drug screening. Therefore, a quantifiable approach was required to determine potential treatment strategies *in vitro* based on morphological damage

identified via image capture. Guided by the experiments described above and with treatment co-applied on the day of transduction, tau-DsRed2 cultures were analysed 3 days and APP-EGFP conditions 5 days post transduction. The proportion of healthy positive neurones (as % of transduced neurones) was identified as the most reliable parameter, due to the detachment of degenerating cells. Compared to EGFP controls ($n=15$ non-washed; $n=10$ washed) APP-EGFP expression induced 73% reduction of this parameter ($p<0.001$, $n=16$; Fig. 5A) and a 50% reduction when an additional wash was conducted ($p=0.001$, $n=11$; Fig. 5B). The concomitant treatment with β- and γ-secretase inhibitors significantly improved the proportion of healthy transduced neurones (BI2: +37% , $n=11$, $p<0.01$; DAPT: +31%, $n=9$; $p<0.01$; Fig. 5A) and reached EGFP control level with the additional wash improvement (BI4: +61%, $n=10$, $p<0.001$; compound E: +46%, $n=12$, $p<0.001$; DAPM: +75%, $n=9$; $p<0.001$; Fig. 5B). This successful treatment via prevention of Aβ formation again indicated intracellular Aβ as the cause of reduced cellular viability and thus also served as a proof-of-principle for the *in vitro* model. Following this, other compounds with proposed neuroprotective properties were tested. The metal-chelating compound clioquinol (CQ) (10 μM; $n=12$) as well as caffeine (50 μM; $n=9$) and lithium (500 μM; $n=9$) prevented APP-EGFP-induced morphological damage (all $p<0.001$). Tau-DsRed2 overexpression reduced the proportion of healthy positive neurones by up to 46% (p's<0.001; Fig. 5C). Short-term application of the anti-aggregation compound MB (0.02%) somewhat ameliorated the damage (+~16%, $p=0.02$, $n=11$) but did not fully restore control levels. Interestingly, the γ-secretase inhibitor DAPM (40 nM; $n=9$) also described as an anti-aggregation compound (Walsh et al., 2002), was more potent in preventing tau-DsRed2-induced damage than MB (+41%, $p<0.001$), while lithium ($n=12$) with its known GSK-3β inhibitory properties had no significant health improving effect on the morphology of tau-DsRed2-expressing neurones (Fig. 5C). As for APP-EGFP, caffeine ($n=9$) was also able to counteract tau-DsRed2 induced damage (+34%, $p=0.03$).

Neurite outgrowth is inhibited by (intracellular) amyloid and tau

So far, data suggested neurite withdrawal as an early and potentially crucial feature of degenerative events in both APP and tau transduced neurones. This was investigated further in neonatal rat DRG cultures, a neuronal preparation especially suitable for studies on axonal outgrowth, guidance and stability (Murray and Shewan, 2008; Plantman et al., 2008) that was found to provide a sensitive assay of gene transduction and quantification, especially for cytoskeletal integrity (Fig. 6). This feature was particularly interesting concerning tau-related damage due to its association with microtubules. Introduction of EGFP did not affect neurite outgrowth (transduction 2.5 h after plating; $n=5$) or maintenance (transduction 24 h post plating; $n=3$; Fig. 7A), while APP-EGFP ($n\geq3$) and tau-DsRed2 ($n\geq4$) decreased both processes ($p<0.01$; Fig. 7B). No significant difference was detected between APP-EGFP and tau-DsRed2 positive neurones at the 24 h time point, while outgrowth (2.5 h time point) was affected more strongly by tau-DsRed2 (74% reduction cf. EGFP; $p<0.001$) than APP-EGFP (44% reduction cf. EGFP; $p=0.005$), corresponding to observations in hippocampal cultures where tau-DsRed2 also had a more aggressive pathology. Treatment of APP-EGFP transduced DRG neurones with BI2 ($n=3$) and tau-DsRed2 transduced neurones with MB ($n=3$) significantly rescued the decrease in neurite outgrowth towards control levels (p's>0.05 cf. controls; Fig. 7C).

Discussion

Adenoviral transduction of primary neuronal cultures with mutated human APP-EGFP or tau-DsRed2 induced early calcium dysregulation, reduced viability in hippocampal neurones and impaired neurite outgrowth in DRG neurones. This approach provides models that

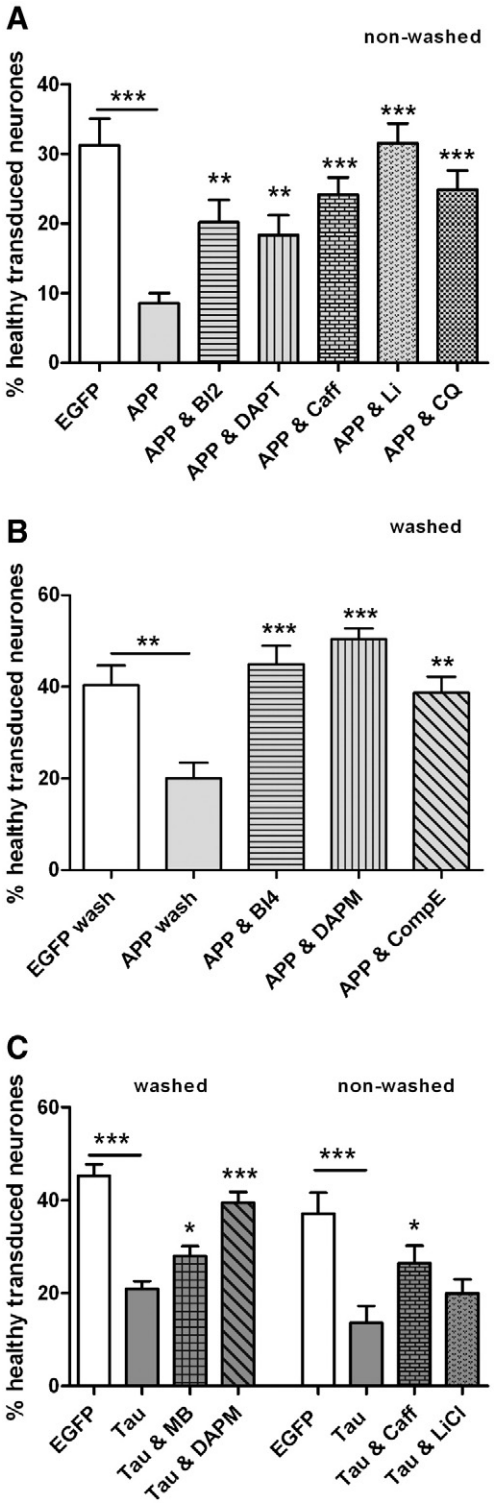

Fig. 5. Morphological damage as a quantitative endpoint for drug testing. Data were quantified as healthy, fluorescence positive neurones out of all positive neurones (% + SEM). (A) Expression of APP-EGFP damaged hippocampal neurones compared to EGFP control (non-washed, for full experimental details, see text). This decrease was reversed by β- (BI2) and γ-secretase inhibitors (DAPT) as well as other neuroprotective compounds. (B) Medium change after one day reduced the morphological damage. In this experimental design β- (BI4) and γ-secretase inhibitors (compound E, DAPM) prevented damage even more efficiently. (C) Tau-transgene induced damage was ameliorated by anti-aggregation compounds MB and DAPM as well as caffeine. $^{*}p<0.05$; $^{**}p<0.01$; $^{***}p<0.001$. Treatment significances indicated above bars are compared to untreated APP-EGFP or tau-DsRed2 conditions, respectively. BI2 = β-secretase inhibitor II; BI4 = β-secretase inhibitor IV; Caff = caffeine; CompE = compound E; CQ = clioquinol; Li = lithium; MB = methylene blue.

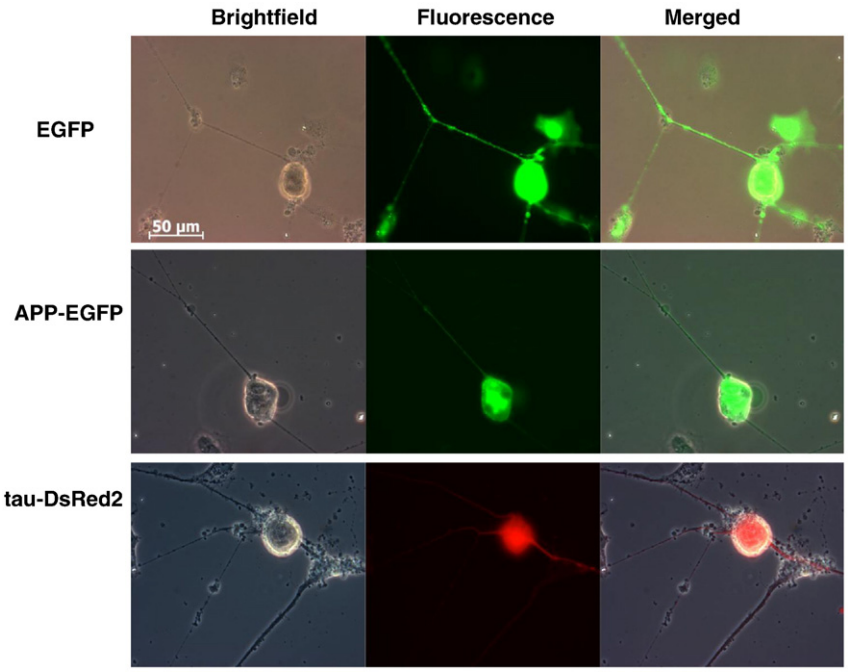

Fig. 6. Viral tranduction of neonatal rat DRG neurones. Depicted are examples of neurons transduced with EGFP, APP-EGFP and tau-DsRed2, with neurites ≥ 3 cell body diameters in length. Scale bar = 50 µm.

allow direct observation and quantification of APP and tau related degenerative mechanisms and testing of prospective treatments. Damage occurred in transduced neurones, but not the surrounding non-transduced neurones (with the exception of late stage tau-DsRed2 transduced cultures), indicative of an intracellular mechanism. In particular for APP and its fast processing, damage is likely due to intracellularly expressed metabolites (e.g. Aβ, C99 or AICD) and not secreted products (Aβ or sAPPα/β). In line with this observation, secreted Aβ levels in our preparation were below the detection limit of ELISAs, as reported previously (Kloskowska et al., 2008), and only low amounts of the strongly expressed $A\beta_{1-40}$ were detected upon immunoprecipitation in cortical cultures (Kienlen-Campard et al., 2002).

As expected from differing protein turnover (tau half life: ~60 h; Poppek et al., 2006 cf. minutes for full-length APP Koo and Squazzo, 1994), as well as protein-specific post-translational modifications and divergent cellular functions, tau-DsRed2 and APP-EGFP induced cellular damage did not follow the same time line and pattern. While tau-DsRed2 had a stronger impact on cell morphology and neurite outgrowth than APP-EGFP, early functional impairments in calcium homoeostasis were evident for both. Cell aggregation in particular, but also the death of non-transduced neurones, only observed for tau-DsRed2, was an indicator of a possible threshold for tau accumulation. Such threshold levels are supported by pilot data from hippocampal cultures transfected via electroporation, where individual neurones transfected with tau-DsRed2 vector had a similar cell death probability but did not affect surrounding neurones (unpublished observation).

Probably related to the complex processing of APP, degenerative events were more variable than for tau: interestingly, early cell death (1 day post transduction) was observed in some APP-EGFP-positive neurones and healthy transduced neurones were still present 5 days post transduction. This may indicate different processing and vulnerabilities to toxic peptides generated in individual neurones, but also suggests delayed expression in subsets of neurones. Varied sensitivity towards APP-EGFP-induced toxicity was also detected in time-lapse imaging: cell death was not confined to bright fluorescent neurones (~high APP-EGFP expression) but occurred in a rather non-stoichiometric manner in cells with high and low fluorescence. This likely reflects cell-type specific vulnerability upon exposure to varying concentrations of APP-derived peptides.

Judging from the sequence of events (neurite withdrawal, shrinkage and fragmentation) APP-EGFP transduced neurones followed an apoptotic-like cell death as observed previously for Aβ treated cells (Kumar-Singh et al., 2002) and APP_{swe} transfected cell lines (Keil et al., 2004). This has been described in AD (Louneva et al., 2008; Stadelmann et al., 1999) although contrasting results have also been presented (Woodhouse et al., 2006). In contrast to APP-EGFP, tau-DsRed2 overexpressing neurones did not follow a typical apoptotic pattern but appeared swollen and distorted. Similar changes in cell shape have been shown in tau-expressing cell lines (Ebneth et al., 1998) with blockage of cellular transport and a resulting misdistribution of organelles, especially mitochondria (Ebneth et al., 1998; Stamer et al., 2002), which increased the vulnerability to oxidative stress. Interestingly, a tau-expressing neuroblastoma cell line was more resistant to apoptosis and tau transgenic mice had lower activation of caspase 3 than tau knock-out mice (H.H. Wang, et al., 2010). This potential anti-apoptotic effect of tau was also observed for Aβ-induced apoptosis in N2a cells (Z.F. Wang, et al., 2010) and may explain the longevity of tangle bearing neurones in AD brains and diverse results on caspases in AD (Raina et al., 2001). Nevertheless, such cells are likely to be functionally impaired. Accordingly, early functional impairments, measured by aberrant calcium homoeostasis and loss of responsiveness to depolarising stimuli, in both APP-EGFP and tau-DsRed2 transgenic cultures indicate an underlying initial calcium dysregulation before manifestation of morphological damage.

With the detection of early and late stage damage, a time line of progressive transgene-specific alterations emerges. In tau-DsRed2 transduced neurones elevated basal intracellular calcium levels and decreased excitability were already evident 2 days post transduction whereas APP-EGFP positive neurones first showed elevated intracellular calcium levels only after 5 days. Together with the earlier onset of morphological damage in hippocampal neurones and stronger impairment of axonal outgrowth in DRG neurones this indicates a stronger toxicity of tau-DsRed2 than APP-EGFP. With regards to the preparations used here, similarities in susceptibility and matching pharmacological

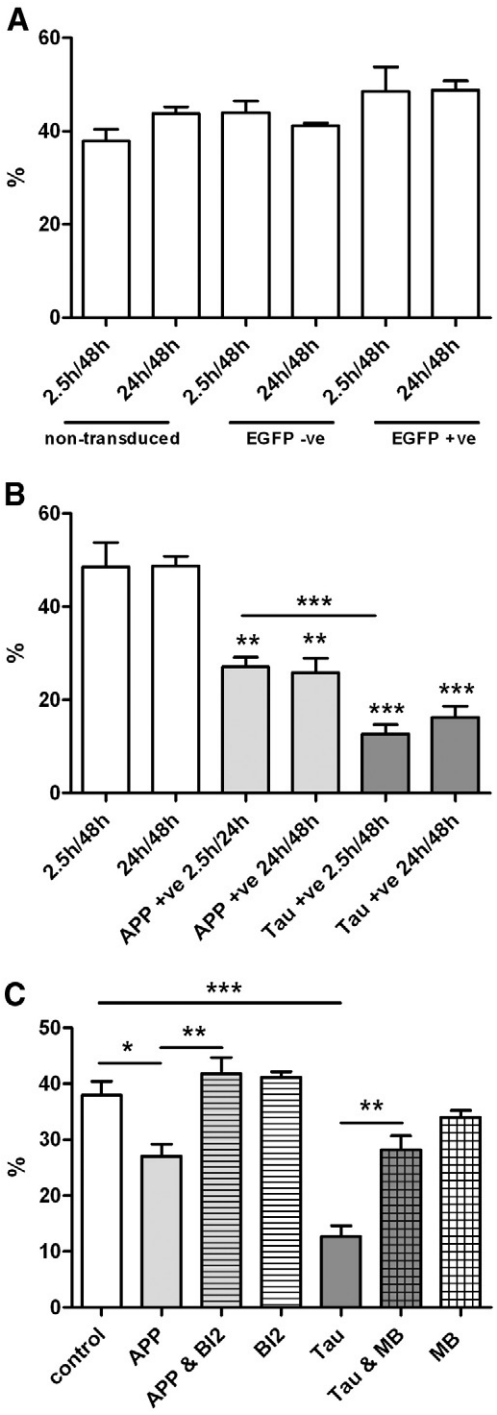

Fig. 7. APP-EGFP and tau-DsRed2 overexpression affects DRG neurite outgrowth and withdrawal. Neurones were transduced either 2.5 h or 24 h post plating for the investigation of neurite outgrowth and withdrawal, respectively, and visualised 48 h post transduction. Data are expressed as neurones with neurites longer than 3 cell body diameters (in % + SEM). (A) Controls: viral transduction with EGFP did not affect neurites (all control conditions are not significantly different from each other). (B) Introduction of APP-EGFP or tau-DsRed2 reduced the proportion of neurite-bearing neurones. Significances indicated above columns are compared to the corresponding EGFP control time point. (C) Rescue of neurite outgrowth (2.5 h time point) in DRG neurones via treatment with β-secretase inhibitor or MB. $^{*}p<0.05$; $^{**}p<0.01$; $^{***}p<0.001$. −ve = negative; + ve = positive; BI2 = β-secretase inhibitor II; MB = methylene blue.

efficacies obtained for DRG vs. hippocampal cultures adds an interesting aspect to the region-specific pathology observed in AD. The damage to DRG neurones induced by APP and tau suggests that PNS neurones are not *per se* protected. Rather, atrophy observed in affected brain areas is likely due to differential expression levels of disease-relevant proteins, and not to the lack of susceptibilities of PNS neurones. DRG preparations can therefore serve as valid models to measure aspects of AD-related cell damage.

The cellular mechanism underlying changed calcium signalling cannot be deduced from the current data but changes in voltage-gated calcium channels (Santos et al., 2009), or NMDA receptor mediated signalling (Shankar et al., 2007; Bi et al., 2002) may be the cause. Damage exerted by intracellular Aβ was previously identified to increase the membrane potential (Hou et al., 2009) and led to rapid apoptotic cell death when directly injected into neurones (Zhang et al., 2002). Taken together, reduced excitability and apoptotic-like cell death in our APP model is congruent with an early dysregulation of calcium homoeostasis leading to apoptosis, while tau overexpression caused morphological distortion after calcium dysregulation. Similar to our data, tau overexpression in organotypic hippocampal slice cultures led to fragmented axonal swellings and slow cell degeneration (Hinners et al., 2008). One underlying effect of these changes may also be increased formation of reactive oxygen species and mitochondrial impairment as seen upon expression of caspase-cleaved tau (Quintanilla et al., 2009).

Neuroprotective compounds for APP-induced damage

Late stage damage, quantified by deteriorated morphology, presented an efficient way for neuroprotection studies. As a proof-of-principle, the model was first tested with secretase inhibitors, interfering with Aβ generation. The successful prevention of morphological damage by all employed β- and γ-secretase inhibitors indicates intracellular Aβ as an underlying cause and demonstrates the usefulness of the cellular model for identifying potential drug candidates. The testing of other such neuroprotective compounds revealed caffeine, lithium and clioquinol as effective against APP-induced damage. The main actions of caffeine are assumed to be mediated via adenosine receptors altering cAMP levels and caffeine has been shown to reduce amyloid levels both *in vitro* and *in vivo* (Arendash et al., 2006, 2009). Reduced activity of the transcription factor NF-κB via c-Raf signalling was identified, and target proteins of NF-κB (BACE1 and presenilin) showed lower expression (Arendash et al., 2006, 2009). The inhibitory action of lithium on GSK-3β (Jope, 2003), a major kinase for tau-phosphorylation, may ameliorate APP toxicity (Iijima et al., 2000; Ryder et al., 2003; but see also comments below regarding tau pathology). Phosphorylation at this position increased BACE1 cleavage and Aβ formation (Lee et al., 2003) as well as the translocation of AICD into the nucleus (Chang et al., 2006), linked with an increased apoptotic function (Ozaki et al., 2006). Clioquinol, on the other hand, is a known metal-chelating agent and redistributes metals in the brain (Lakatos et al., 2010). A new derivative (PTB2) reduced $A\beta_{1-42}$ levels and improved cognitive deficits in a Phase II clinical trial (Lannfelt et al., 2008; Faux et al., 2010). The underlying cellular pathway is not identified yet but sequestration of neurotoxic metals (e.g. Zn, Al, Cu; Platt, 2008) may have prevented oxidative damage (Kong et al., 2008) and/or formation of more toxic oligomeric Aβ species.

Neuroprotective compounds for tau-induced damage

While MB treatment did not significantly alter calcium responses in tau transduced neurones, the damage in cell morphology was ameliorated. MB has been shown to reduce tau-tau binding *in vitro* (Wischik et al., 1996) and interfere with heparin-induced tau filament formation (Taniguchi et al., 2005; Hattori et al., 2008), but also has a variety of other unrelated functions such as electron acceptor and donor (Oz et al., 2009) and thus has been shown to reduce oxidative stress (Atamna et al., 2008) and increase cytochrome *C* oxidase activity (Callaway et al., 2004). This property likely plays a role in the ameliorating effect in the tau transduced neurones. Because of the described anti-aggregation properties of the γ-secretase inhibitor

DAPM this compound was also tested and found more efficient in preventing tau-induced damage than MB, indicative of aggregation as a contributing factor.

Additionally, lithium and caffeine were selected for treatment. Lithium was chosen due to its inhibitory effect on tau phosphorylation and the reduction in NFT formation in short-term treatment of tau-transgenic animals (Leroy et al., 2010). Despite previous reports on lithium's inhibitory effect on the major tau kinase, GSK-3β (Jope, 2003), treatment did not ameliorate the damage. While phosphorylation levels of tau protein may not have been sufficiently reduced to prevent damage in our preparation, divergent effects of lithium on cognitive and biochemical parameters are not unprecedented. Lithium treatment of transgenic mice did reduce tau phosphorylation but neither influenced Aβ levels nor improved working memory deficits (Caccamo et al., 2007). Equally, only some clinical trials found benefits for cognition (Leyhe et al., 2009), while others reported no improvement (Hampel et al., 2009). This indicates different roles of lithium as a neuroprotective agent that could be unrelated to tau pathology. Interestingly, as for APP the psychoactive stimulant caffeine yielded protection against tau-induced damage. The inhibition of GSK-3β by PKA is thus unlikely to be the sole component against tau pathology. So far, no direct action of caffeine on the phosphorylation or aggregation of tau has been reported, although new evidence in a rabbit model of sporadic AD showed a reduction in cholesterol-induced phospho-tau levels after oral caffeine treatment (Prasanthi et al., 2010). Nevertheless, the exact underlying mechanism(s) of caffeine's action remain to be identified, but its consistently reported protective effect in AD models is compelling.

The current drug studies, based on concurrent application of treatments and transduction, present a protection-based approach that can now be expanded to determine beneficial actions for recovery after pathology onset, and to investigate other contributing factors, such as anti-oxidants and environmental stressors. Though obvious differences to the human condition must be acknowledged, our approach provides a convenient test bed to further explore and compare cellular mechanisms underlying APP and tau pathology, and identify treatments to prevent respective cellular damage.

Supplementary materials related to this article can be found online at doi:10.1016/j.expneurol.2011.01.018.

Acknowledgments

The authors would like to thank the University of Aberdeen Bone Group for the permission to use the category 2 facility to work with the adenoviruses. SS was in part supported by a Sixth Century studentship.

References

Arendash, G.W., Schleif, W., Rezai-Zadeh, K., Jackson, E.K., Zacharia, L.C., Cracchiolo, J.R., Shippy, D., Tan, J., 2006. Caffeine protects Alzheimer's mice against cognitive impairment and reduces brain beta-amyloid production. Neuroscience 142, 941–952.

Arendash, G.W., Mori, T., Cao, C., Mamcarz, M., Runfeldt, M., Dickson, A., Rezai-Zadeh, K., Tan, J., Citron, B.A., Lin, X., Echeverria, V., Potter, H., 2009. Caffeine reverses cognitive impairment and decreases brain amyloid-beta levels in aged Alzheimer's disease mice. J. Alzheimers Dis. 17, 661–680.

Atamna, H., Nguyen, A., Schultz, C., Boyle, K., Newberry, J., Kato, H., Ames, B.N., 2008. Methylene blue delays cellular senescence and enhances key mitochondrial biochemical pathways. FASEB J. 22, 703–712.

Bi, X., Gall, C.M., Zhou, J., Lynch, G., 2002. Uptake and pathogenic effects of amyloid beta peptide 1–42 are enhanced by integrin antagonists and blocked by NMDA receptor antagonists. Neuroscience 112, 827–840.

Caccamo, A., Oddo, S., Tran, L.X., LaFerla, F.M., 2007. Lithium reduces tau phosphorylation but not A beta or working memory deficits in a transgenic model with both plaques and tangles. Am. J. Pathol. 170, 1669–1675.

Callaway, N.L., Riha, P.D., Bruchey, A.K., Munshi, Z., Gonzalez-Lima, F., 2004. Methylene blue improves brain oxidative metabolism and memory retention in rats. Pharmacol. Biochem. Behav. 77, 175–181.

Chang, K.A., Kim, H.S., Ha, T.Y., Ha, J.W., Shin, K.Y., Jeong, Y.H., Lee, J.P., Park, C.H., Kim, S., Baik, T.K., Suh, Y.H., 2006. Phosphorylation of amyloid precursor protein (APP) at Thr668 regulates the nuclear translocation of the APP intracellular domain and induces neurodegeneration. Mol. Cell. Biol. 26, 4327–4338.

Citron, M., Vigo-Pelfrey, C., Teplow, D.B., Miller, C., Schenk, D., Johnston, J., Winblad, B., Venizelos, N., Lannfelt, L., Selkoe, D.J., 1994. Excessive production of amyloid beta-protein by peripheral cells of symptomatic and presymptomatic patients carrying the Swedish familial Alzheimer disease mutation. Proc. Natl Acad. Sci. USA 91, 11993–11997.

Cleary, J.P., Walsh, D.M., Hofmeister, J.J., Shankar, G.M., Kuskowski, M.A., Selkoe, D.J., Ashe, K.H., 2005. Natural oligomers of the amyloid-beta protein specifically disrupt cognitive function. Nat. Neurosci. 8, 79–84.

Ebneth, A., Godemann, R., Stamer, K., Illenberger, S., Trinczek, B., Mandelkow, E., 1998. Overexpression of tau protein inhibits kinesin-dependent trafficking of vesicles, mitochondria, and endoplasmic reticulum: implications for Alzheimer's disease. J. Cell Biol. 143, 777–794.

Faux, N.G., Ritchie, C.W., Gunn, A., Rembach, A., Tsatsanis, A., Bedo, J., Harrison, J., Lannfelt, L., Blennow, K., Zetterberg, H., Ingelsson, M., Masters, C.L., Tanzi, R.E., Cummings, J.L., Herd, C.M., Bush, A.I., 2010. PBT2 rapidly improves cognition in Alzheimer's disease: additional phase II analyses. J. Alzheimers Dis. 20, 509–516.

Goedert, M., 2005. Tau gene mutations and their effects. Mov. Disord. 20 (Suppl 12), S45–S52.

Goldsbury, C., Mocanu, M.-M., Thies, E., Kaether, C., Haass, C., Keller, P., Biernat, J., Mandelkow, E., Mandelkow, E.-M., 2006. Inhibition of APP trafficking by Tau protein does not increase the generation of amyloid-beta peptides. Traffic 7, 873–888.

Gralle, M., Ferreira, S.T., 2007. Structure and function of the human amyloid precursor protein: the whole is more than the sum of its parts. Prog. Neurobiol. 82, 11–32.

Hampel, H., Ewers, M., Burger, K., Annas, P., Mortberg, A., Bogstedt, A., Frolich, L., Schroder, J., Schonknecht, P., Riepe, M.W., Kraft, I., Gasser, T., Leyhe, T., Moller, H.J., Kurz, A., Basun, H., 2009. Lithium trial in Alzheimer's disease: a randomized, single-blind, placebo-controlled, multicenter 10-week study. J. Clin. Psychiatry 70, 922–931.

Hattori, M., Sugino, E., Minoura, K., In, Y., Sumida, M., Taniguchi, T., Tomoo, K., Ishida, T., 2008. Different inhibitory response of cyanidin and methylene blue for filament formation of tau microtubule-binding domain. Biochem. Biophys. Res. Commun. 374, 158–163.

Hinners, I., Hill, A., Otto, U., Michalsky, A., Mack, T.G., Striggow, F., 2008. Tau kinase inhibitors protect hippocampal synapses despite of insoluble tau accumulation. Mol. Cell. Neurosci. 37, 559–567.

Hou, J.F., Cui, J., Yu, L.C., Zhang, Y., 2009. Intracellular amyloid induces impairments on electrophysiological properties of cultured human neurons. Neurosci. Lett. 462, 294–299.

Iijima, K., Ando, K., Takeda, S., Satoh, Y., Seki, T., Itohara, S., Greengard, P., Kirino, Y., Nairn, A.C., Suzuki, T., 2000. Neuron-specific phosphorylation of Alzheimer's beta-amyloid precursor protein by cyclin-dependent kinase 5. J. Neurochem. 75, 1085–1091.

Jope, R.S., 2003. Lithium and GSK-3: one inhibitor, two inhibitory actions, multiple outcomes. Trends Pharmacol. Sci. 24, 441–443.

Keil, U., Bonert, A., Marques, C.A., Scherping, I., Weyermann, J., Strosznajder, J.B., Muller-Spahn, F., Haass, C., Czech, C., Pradier, L., Muller, W.E., Eckert, A., 2004. Amyloid beta-induced changes in nitric oxide production and mitochondrial activity lead to apoptosis. J. Biol. Chem. 279, 50310–50320.

Kienlen-Campard, P., Miolet, S., Tasiaux, B., Octave, J.N., 2002. Intracellular amyloid-beta 1–42, but not extracellular soluble amyloid-beta peptides, induces neuronal apoptosis. J. Biol. Chem. 277, 15666–15670.

Kloskowska, E., Malkiewicz, K., Winblad, B., Benedikz, E., Bruton, J.D., 2008. APPswe mutation increases the frequency of spontaneous Ca2+-oscillations in rat hippocampal neurons. Neurosci. Lett. 436, 250–254.

Kong, G.K., Miles, L.A., Crespi, G.A., Morton, C.J., Ng, H.L., Barnham, K.J., McKinstry, W.J., Cappai, R., Parker, M.W., 2008. Copper binding to the Alzheimer's disease amyloid precursor protein. Eur. Biophys. J. 37, 269–279.

Koo, E.H., Squazzo, S.L., 1994. Evidence that production and release of amyloid beta-protein involves the endocytic pathway. J. Biol. Chem. 269, 17386–17389.

Koss, D.J., Hindley, K.P., Riedel, G., Platt, B., 2007. Modulation of hippocampal calcium signalling and plasticity by serine/threonine protein phosphatases. J. Neurochem. 102, 1009–1023.

Kumar-Singh, S., Julliams, A., Nuydens, R., Ceuterick, C., Labeur, C., Serneels, S., Vennekens, K., Van Osta, P., Geerts, H., De Strooper, B., Van Broeckhoven, C., 2002. In vitro studies of Flemish, Dutch, and wild-type beta-amyloid provide evidence for two-staged neurotoxicity. Neurobiol. Dis. 11, 330–340.

Lakatos, A., Zsigo, E., Hollender, D., Nagy, N.V., Fulop, L., Simon, D., Bozso, Z., Kiss, T., 2010. Two pyridine derivatives as potential Cu(II) and Zn(II) chelators in therapy for Alzheimer's disease. Dalton Trans. 39, 1302–1315.

Lannfelt, L., Blennow, K., Zetterberg, H., Batsman, S., Ames, D., Harrison, J., Masters, C.L., Targum, S., Bush, A.I., Murdoch, R., Wilson, J., Ritchie, C.W., PBT2-201-EURO study group, 2008. Safety, efficacy, and biomarker findings of PBT2 in targeting Abeta as a modifying therapy for Alzheimer's disease: a phase IIa, double-blind, randomised, placebo-controlled trial. Lancet Neurol. 7, 779–786.

Lee, M.S., Kao, S.C., Lemere, C.A., Xia, W., Tseng, H.C., Zhou, Y., Neve, R., Ahlijanian, M.K., Tsai, L.H., 2003. APP processing is regulated by cytoplasmic phosphorylation. J. Cell Biol. 163, 83–95.

Leroy, K., Ando, K., Heraud, C., Yilmaz, Z., Authelet, M., Boeynaems, J.M., Buee, L., De Decker, R., Brion, J.P., 2010. Lithium treatment arrests the development of neurofibrillary tangles in mutant tau transgenic mice with advanced neurofibrillary pathology. J. Alzheimers Dis. 19, 705–719.

Lesne, S., Koh, M.T., Kotilinek, L., Kayed, R., Glabe, C.G., Yang, A., Gallagher, M., Ashe, K.H., 2006. A specific amyloid-beta protein assembly in the brain impairs memory. Nature 440, 352–357.

Leyhe, T., Eschweiler, G.W., Stransky, E., Gasser, T., Annas, P., Basun, H., Laske, C., 2009. Increase of BDNF serum concentration in lithium treated patients with early Alzheimer's disease. J. Alzheimers Dis. 16, 649–656.

Lo, D.C., McAllister, A.K., Katz, L.C., 1994. Neuronal transfection in brain slices using particle-mediated gene transfer. Neuron 13, 1263–1268.
Louneva, N., Cohen, J.W., Han, L.Y., Talbot, K., Wilson, R.S., Bennett, D.A., Trojanowski, J.Q., Arnold, S.E., 2008. Caspase-3 is enriched in postsynaptic densities and increased in Alzheimer's disease. Am. J. Pathol. 173, 1488–1495.
Luo, J.J., Wallace, W., Riccioni, T., Ingram, D.K., Roth, G.S., Kusiak, J.W., 1999. Death of PC12 cells and hippocampal neurons induced by adenoviral-mediated FAD human amyloid precursor protein gene expression. J. Neurosci. Res. 55, 629–642.
Macq, A.F., Czech, C., Essalmani, R., Brion, J.P., Maron, A., Mercken, L., Pradier, L., Octave, J.N., 1998. The long term adenoviral expression of the human amyloid precursor protein shows different secretase activities in rat cortical neurons and astrocytes. J. Biol. Chem. 273, 28931–28936.
Masumura, M., Hata, R., Nishimura, I., Uetsuki, T., Sawada, T., Yoshikawa, K., 2000. Caspase-3 activation and inflammatory responses in rat hippocampus inoculated with a recombinant adenovirus expressing the Alzheimer amyloid precursor protein. Brain Res. Mol. Brain Res. 80, 219–227.
Mc Donald, J.M., Savva, G.M., Brayne, C., Welzel, A.T., Forster, G., Shankar, G.M., Selkoe, D.J., Ince, P.G., Walsh, D.M., Medical Research Council Cognitive Function and Ageing Study, 2010. The presence of sodium dodecyl sulphate-stable Abeta dimers is strongly associated with Alzheimer-type dementia. Brain 133, 1328–1341.
Murray, A.J., Shewan, D.A., 2008. Epac mediates cyclic AMP-dependent axon growth, guidance and regeneration. Mol. Cell. Neurosci. 38, 578–588.
Murray, A.J., Peace, A.G., Shewan, D.A., 2009. cGMP promotes neurite outgrowth and growth cone turning and improves axon regeneration on spinal cord tissue in combination with cAMP. Brain Res. 1294, 12–21.
Necula, M., Breydo, L., Milton, S., Kayed, R., van der Veer, W.E., Tone, P., Glabe, C.G., 2007. Methylene blue inhibits amyloid Abeta oligomerization by promoting fibrillization. Biochemistry 46, 8850–8860.
Niewiadomska, G., Baksalerska-Pazera, M., Riedel, G., 2005. Altered cellular distribution of phospho-tau proteins coincides with impaired retrograde axonal transport in neurons of aged rats. Ann. NY Acad. Sci. 1048, 287–295.
Nishimura, I., Uetsuki, T., Dani, S.U., Ohsawa, Y., Saito, I., Okamura, H., Uchiyama, Y., Yoshikawa, K., 1998. Degeneration in vivo of rat hippocampal neurons by wild-type Alzheimer amyloid precursor protein overexpressed by adenovirus-mediated gene transfer. J. Neurosci. 18, 2387–2398.
Oz, M., Lorke, D.E., Petroianu, G.A., 2009. Methylene blue and Alzheimer's disease. Biochem. Pharmacol. 78, 927–932.
Ozaki, T., Li, Y., Kikuchi, H., Tomita, T., Iwatsubo, T., Nakagawara, A., 2006. The intracellular domain of the amyloid precursor protein (AICD) enhances the p53-mediated apoptosis. Biochem. Biophys. Res. Commun. 351, 57–63.
Paglini, G., Peris, L., Mascotti, F., Quiroga, S., Caceres, A., 2000. Tau protein function in axonal formation. Neurochem. Res. 25, 37–42.
Plantman, S., Patarroyo, M., Fried, K., Domogatskaya, A., Tryggvason, K., Hammarberg, H., Cullheim, S., 2008. Integrin–laminin interactions controlling neurite outgrowth from adult DRG neurons in vitro. Mol. Cell. Neurosci. 39, 50–62.
Platt, B., 2008. Metals, neurotoxicity and neurodegenerative disorders. In: Merce, A.L.R., Felcman, J., Recio, M.A.L. (Eds.), Molecular and Supramolecular Bioinorganic Chemistry: Applications in Medical Sciences. Nova Science Publishers, New York, pp. 69–81.
Poppek, D., Keck, S., Ermak, G., Jung, T., Stolzing, A., Ullrich, O., Davies, K.J., Grune, T., 2006. Phosphorylation inhibits turnover of the tau protein by the proteasome: influence of RCAN1 and oxidative stress. Biochem. J. 400, 511–520.
Prasanthi, R.J., Dasari, B., Marwarha, G., Larson, T., Chen, X., Geiger, J.D., Ghribi, O., 2010. Caffeine protects against oxidative stress and Alzheimer's disease-like pathology in rabbit hippocampus induced by cholesterol-enriched diet. Free Radic. Biol. Med. 49, 1212–1220.
Querfurth, H.W., LaFerla, F.M., 2010. Mechanisms of disease: Alzheimer's disease. N. Engl. J. Med. 326, 329–344.
Quintanilla, R.A., Matthews-Roberson, T.A., Dolan, P.J., Johnson, G.V., 2009. Caspase-cleaved tau expression induces mitochondrial dysfunction in immortalized cortical neurons: implications for the pathogenesis of Alzheimer disease. J. Biol. Chem. 284, 18754–18766.
Raina, A.K., Hochman, A., Zhu, X., Rottkamp, C.A., Nunomura, A., Siedlak, S.L., Boux, H., Castellani, R.J., Perry, G., Smith, M.A., 2001. Abortive apoptosis in Alzheimer's disease. Acta Neuropathol. 101, 305–310.
Ryan, D., Drysdale, A.J., Lafourcade, C., Pertwee, R.G., Platt, B., 2009. Cannabidiol targets mitochondria to regulate intracellular Ca^{2+} levels. J. Neurosci. 29, 2053–2063.
Ryder, J., Su, Y., Liu, F., Li, B., Zhou, Y., Ni, B., 2003. Divergent roles of GSK3 and CDK5 in APP processing. Biochem. Biophys. Res. Commun. 312, 922–929.
Santos, S.F., Pierrot, N., Morel, N., Gailly, P., Sindic, C., Octave, J.N., 2009. Expression of human amyloid precursor protein in rat cortical neurons inhibits calcium oscillations. J. Neurosci. 29, 4708–4718.
Selkoe, D.J., 2001. Alzheimer's disease: genes, proteins, and therapy. Physiol. Rev. 81, 741–766.
Shankar, G.M., Bloodgood, B.L., Townsend, M., Walsh, D.M., Selkoe, D.J., Sabatini, B.L., 2007. Natural oligomers of the Alzheimer amyloid-beta protein induce reversible synapse loss by modulating an NMDA-type glutamate receptor-dependent signaling pathway. J. Neurosci. 27, 2866–2875.
Sinha, S., Lieberburg, I., 1999. Cellular mechanisms of beta-amyloid production and secretion. Proc. Natl Acad. Sci. USA 96, 11049–11053.
Stadelmann, C., Deckwerth, T.L., Srinivasan, A., Bancher, C., Bruck, W., Jellinger, K., Lassmann, H., 1999. Activation of caspase-3 in single neurons and autophagic granules of granulovacuolar degeneration in Alzheimer's disease. Evidence for apoptotic cell death. Am. J. Pathol. 155, 1459–1466.
Stamer, K., Vogel, R., Thies, E., Mandelkow, E., Mandelkow, E.M., 2002. Tau blocks traffic of organelles, neurofilaments, and APP vesicles in neurons and enhances oxidative stress. J. Cell Biol. 156, 1051–1063.
Stoppelkamp, S., Riedel, G., Platt, B., 2010. Culturing conditions determine neuronal and glial excitability. J. Neurosci. Meth. 194, 132–138.
Stutzmann, G.E., 2007. The pathogenesis of Alzheimers disease is it a lifelong "calciumopathy"? Neuroscientist 13, 546–559.
Taniguchi, S., Suzuki, N., Masuda, M., Hisanaga, S., Iwatsubo, T., Goedert, M., Hasegawa, M., 2005. Inhibition of heparin-induced tau filament formation by phenothiazines, polyphenols, and porphyrins. J. Biol. Chem. 280, 7614–7623.
Tominaga, K., Uetsuki, T., Ogura, A., Yoshikawa, K., 1997. Glutamate responsiveness enhanced in neurones expressing amyloid precursor protein. NeuroReport 8, 2067–2072.
Tominaga-Yoshino, K., Uetsuki, T., Yoshikawa, K., Ogura, A., 2001. Neurotoxic and neuroprotective effects of glutamate are enhanced by introduction of amyloid precursor protein cDNA. Brain Res. 918, 121–130.
Walsh, D.M., Selkoe, D.J., 2004. Deciphering the molecular basis of memory failure in Alzheimer's disease. Neuron 44, 181–193.
Walsh, D.M., Klyubin, I., Fadeeva, J.V., Cullen, W.K., Anwyl, R., Wolfe, M.S., Rowan, M.J., Selkoe, D.J., 2002. Naturally secreted oligomers of amyloid beta protein potently inhibit hippocampal long-term potentiation in vivo. Nature 416, 535–539.
Wang, H.H., Li, H.L., Liu, R., Zhang, Y., Liao, K., Wang, Q., Wang, J.Z., Liu, S.J., 2010a. Tau overexpression inhibits cell apoptosis with the mechanisms involving multiple viability-related factors. J. Alzheimers Dis. 21, 167–179.
Wang, Z.F., Yin, J., Zhang, Y., Zhu, L.Q., Tian, Q., Wang, X.C., Li, H.L., Wang, J.Z., 2010b. Overexpression of tau proteins antagonizes amyloid-beta-potentiated apoptosis through mitochondria–caspase-3 pathway in N2a cells. J. Alzheimers Dis. 20, 145–157.
Wischik, C.M., Edwards, P.C., Lai, R.Y., Roth, M., Harrington, C.R., 1996. Selective inhibition of Alzheimer disease-like tau aggregation by phenothiazines. Proc. Natl Acad. Sci. USA 93, 11213–11218.
Woodhouse, A., Dickson, T.C., West, A.K., McLean, C.A., Vickers, J.C., 2006. No difference in expression of apoptosis-related proteins and apoptotic morphology in control, pathologically aged and Alzheimer's disease cases. Neurobiol. Dis. 22, 323–333.
Yuan, H., Zhai, P., Anderson, L.M., Pan, J., Thimmapaya, B., Koo, E.H., Marquez-Sterling, N.R., 1999. Recombinant adenovirus is an appropriate vector for endocytotic protein trafficking studies in cultured neurons. J. Neurosci. Meth. 88, 45–54.
Zhang, Y., McLaughlin, R., Goodyer, C., LeBlanc, A., 2002. Selective cytotoxicity of intracellular amyloid beta peptide1–42 through p53 and Bax in cultured primary human neurons. J. Cell Biol. 156, 519–529.